

Heavy element abundances in planetary nebulae: A theorist's perspective

Amanda I. Karakas^{A,C} and Maria Lugaro^B

^A Research School of Astronomy & Astrophysics, Mount Stromlo Observatory, Cotter Road Weston Creek, ACT 2611, Australia

^B Centre for Stellar and Planetary Astrophysics, Monash University, PO Box 28M, Clayton VIC 3800, Australia

^C Email: akarakas@mso.anu.edu.au

Abstract: The determination of heavy element abundances from planetary nebula (PN) spectra provides an exciting opportunity to study the nucleosynthesis occurring in the progenitor asymptotic giant branch (AGB) star. We perform post-processing calculations on AGB models of a large range of mass and metallicity to obtain predictions for the production of neutron-capture elements up to the first *s*-process peak at strontium. We find that solar metallicity intermediate-mass AGB models provide a reasonable match to the heavy element composition of Type I PNe. Likewise, many of the Se and Kr enriched PNe are well fitted by lower mass models with solar or close-to-solar metallicities. However the most Kr-enriched objects, and the PN with sub-solar Se/O ratios are difficult to explain with AGB nucleosynthesis models. Furthermore, we compute *s*-process abundance predictions for low-mass AGB models of very low metallicity ($\text{Fe}/\text{H} \approx -2.3$) using both scaled solar and an α -enhanced initial composition. For these models, O is dredged to the surface, which means that abundance ratios measured relative to this element (e.g., X/O) do not provide a reliable measure of initial abundance ratios, or of production within the star owing to internal nucleosynthesis.

Keywords: stars: AGB and post-AGB — abundances — ISM: abundances — planetary nebulae: general

1 Introduction

After the thermally-pulsing AGB (TP-AGB) phase is terminated, low to intermediate-mass stars (~ 0.8 to $8M_{\odot}$) evolve at near constant luminosity to become post-AGB objects. If the ejected envelope has sufficient time to become ionized by the hot central star before dissipating, then the object will also be observed as a planetary nebula (PN). For recent reviews of TP-AGB and post-AGB stars, see Herwig (2005) and van Winckel (2003), respectively. The ionised nebula is comprised of material from the convective envelope that once surrounded the core, hence, nebular abundances may reveal information about the efficiency of mixing events and chemical processing that took place during previous evolutionary phases, in addition to the initial composition of the parent star (e.g., Dopita et al. 1997; Magrini et al. 2009).

During the life of a star, mixing between the nuclear-processed core and envelope may occur, and this has the effect of enriching the surface composition in the products of H-burning (first and second dredge-up; hot bottom burning), and He-burning (the third dredge-up). Note that the first dredge-up occurs after core H-exhaustion, whereas the second dredge-up after core He-exhaustion. Both the third dredge up (TDU) and hot bottom burning (HBB) occur during the TP-AGB phase. We refer the reader to, e.g., Boothroyd & Sackmann (1999) for details on the first and second dredge up.

A TP-AGB star is characterised by two nuclear

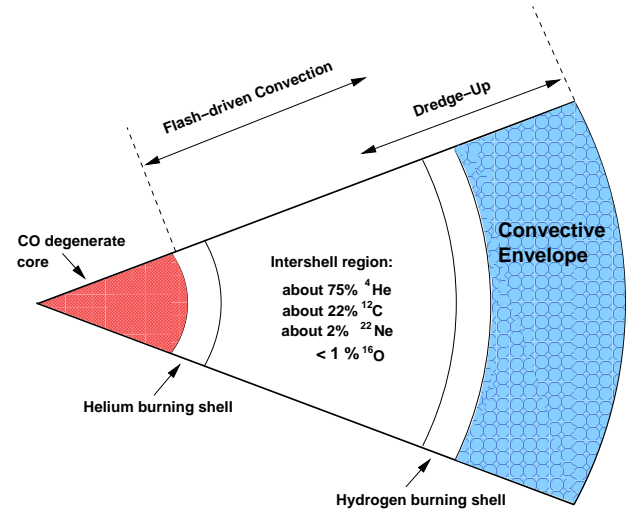


Figure 1: Schematic structure of an AGB star.

burning shells above a degenerate C-O core, surrounded by a deep convective envelope (see Fig. 1). The TDU mixes material from the He-intershell to the envelope. This material is composed primarily of ^4He and ^{12}C , along with trace quantities of heavy elements produced by the *slow* neutron capture process (the *s*-process). The TDU may occur after each instability of the helium shell, slowly enriching the envelope in carbon and heavy elements. HBB occurs in intermediate-mass AGB stars (~ 4 to $8M_{\odot}$) when the base of the convective envelope can dip into the top of the hydrogen burning shell.

Abundances derived from PN spectra provide a complimentary data set to the abundances derived from the spectra of cool evolved stars. For example, the elemental abundances of He, Ne, and Ar can be obtained, along with the abundances of C, N, O, S, and Cl (Aller & Czyzak 1983; Stanghellini et al. 2000; Leisy & Demmele 2006). Recent observations have also revealed that some PNe are enriched in heavy elements that can be produced by the *s*-process including Ge, Se, Kr, Xe, and Ba (Sharpee et al. 2007; Sterling & Dinerstein 2008, hereafter SD08). SD08 obtained Se and Kr abundances for 120 Galactic PNe, and investigated trends between *s*-process enrichments and PN morphology and other nebular and stellar characteristics. It was found that while some PN have large enrichments of Se and Kr (e.g., $[\text{Se}/\text{Kr}/\text{O}] > 1$), Type I PN have lower *s*-process abundances, on average, than the sample as a whole.

In Karakas et al. (2009) we compared nucleosynthesis predictions from models of intermediate-mass AGB stars to the results from SD08. Here we briefly summarize the results from Karakas et al. (2009), and provide new results for lower mass AGB models of solar and halo compositions.

2 Type I Planetary Nebula

The aims of Karakas et al. (2009) were to compare the *s*-process predictions from intermediate-mass AGB stars to the Se and Kr compositions of the Type I PN identified in the SD08 sample. Such a comparison may be used to constrain the efficiency of the TDU in AGB models, which is not well determined. Also this information may help elucidate to what extent intermediate-mass AGB stars contribute to the Galactic inventory of *s*-process elements. The motivation to use Type I PN comes from their high He/H and N/O ratios characteristic of proton-capture nucleosynthesis (Stanghellini et al. 2006), as well as spatial distributions and kinematics indicative of a young population (Corradi & Schwarz 1995) with initial masses between ≈ 2.5 to $6M_{\odot}$.

Furthermore, we had also hoped to identify the neutron source(s) operating in intermediate-mass AGB stars. In low-mass stars it has been shown that the $^{13}\text{C}(\alpha, n)^{16}\text{O}$ reaction is the dominant source of neutrons, whereas the $^{22}\text{Ne}(\alpha, n)^{25}\text{Mg}$ reaction only plays a minor role (Lambert et al. 1995; Gallino et al. 1998). The $^{22}\text{Ne}(\alpha, n)$ reaction has been suggested as the dominant neutron source in intermediate-mass AGB stars

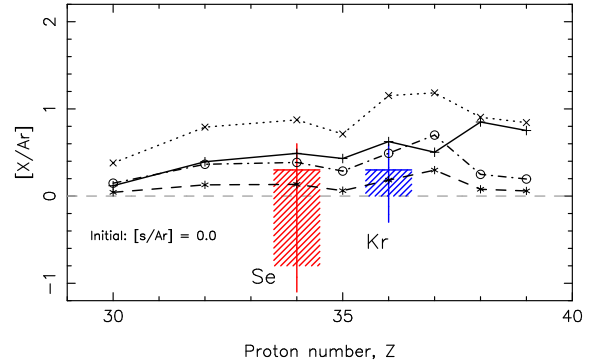


Figure 2: The surface abundances of neutron-capture elements around the first *s*-process peak. The solid line indicates abundances from the $3M_{\odot}$, $Z = 0.02$ model, the dashed line abundances from the $6.5M_{\odot}$, $Z = 0.02$ model, the dot-dashed line abundances from the $5M_{\odot}$, $Z = 0.008$, and the dotted line abundances from the $5M_{\odot}$, $Z = 0.004$ model. Abundances are taken at the tip of the TP-AGB, after the last computed thermal pulse. The boxes represent the range of observed Se and Kr abundances for Type I PNe, see the text for details.

(Truran & Iben 1977; García-Hernández et al. 2006). The *s*-process abundance pattern that results from each reaction is quite different, owing to differing time-scales over which the neutrons are released along with maximum neutron densities that vary by orders of magnitude: $\sim 10^8$ for the ^{13}C reaction compared to $\sim 10^{13}$ neutrons per cm^{-3} for ^{22}Ne . One important result, for example, is the prediction of low Rb/Sr ratios in low-mass AGB stars, which has been observationally verified (e.g., Lambert et al. 1995).

The details of the stellar models and nucleosynthesis calculations have been discussed in detail in Karakas et al. (2009) and Karakas & Lattanzio (2007). Here we summarize the main findings. It is important to point out that only models with HBB ($> 4M_{\odot}$) would be observed as Type I PNe, whereas observations put the minimum mass at $\sim 2.5M_{\odot}$. Clearly, the lowest mass range would require either rapid stellar rotation, extra mixing, and/or the effect of a binary companion to assist in producing the Type I composition.

In Karakas et al. (2009) we found that the HBB AGB models of solar or near solar metallicity (in particular $Z = 0.02$ and 0.008) were a reasonable match to the Se and Kr abundance distribution of the Type I PNe, see Fig. 2. In Fig. 2 the abundances are shown as $[\text{X}/\text{Ar}]$ ratios, and are plotted as a function of proton number, Z . The hatched boxes around the elements Se and Kr indicate the range of the Type I PN abundances from the SD08 sample, with the solid vertical line extending the boxes by an extra 0.3 dex, indicative of the typical errors.

The intermediate-mass low metallicity models ($Z = 0.004$) produced Se and Kr abundances that were in excess of the Type I PN abundances (see the dotted line in Fig. 2), indicating that the PN we see today did not form from such low-metallicity objects. This

result is consistent with the PN evolving from a young, disk population. The $3M_{\odot}$ models of solar metallicity were a marginal fit to the Se and Kr data for Type I PNe. The $3M_{\odot}$ models became carbon rich and we would not predict them to be observed as Type I objects with high He/H and N/O ratios. Rapid rotation during the main sequence could, however, bring some CN-processed material to the surface.

Binarity may be the condition necessary for shaping bipolar PNe (and perhaps all PNe) (Moe & De Marco 2006). Many, but not all, Type I PNe are also bipolar in shape. If binary interactions can produce a Type I composition, then this may lead to the TP-AGB phase being terminated early, before many thermal pulses have occurred. Hence the prediction would be for lower *s*-process elements to be produced, on average, compared to star that evolve to the tip of the AGB phase. This would also be consistent with the observations of no *s*-process enrichment observed in Type I PNe.

3 Se and Kr abundances in low-mass AGB stars

In Fig. 3 we show the surface abundances of Zn, Ge, Se, Br, Kr, and Sr at the tip of the AGB phase for three low-mass AGB models. The solid line represents the abundances from the $3M_{\odot}$, $Z = 0.02$ model, the dashed line abundances for the $2.1M_{\odot}$, $Z = 0.008$ model, and the dot-dashed line abundances for the $2.5M_{\odot}$, $Z = 0.008$ model. Abundances are shown as $[X/O]$ ratios. The hatched boxes around the elements Se and Kr indicate the range of the PN abundances for the full sample from SD08, where the solid vertical line extending the boxes by an extra 0.3 dex, indicative of the typical errors. All models include a partial mixing zone of $0.002M_{\odot}$. This mixing zone produces a ^{13}C pocket during the interpulse period, allowing the reaction $^{13}\text{C}(\alpha, n)^{16}\text{O}$ to release free neutrons. Note that models without partial mixing zones result in no enrichment of *s*-process elements (e.g., Karakas et al. 2007). We refer the reader to Busso et al. (1999) and Herwig (2005) for detailed discussion about the formation of ^{13}C pockets and related uncertainties.

From Fig. 3 we see that the solar metallicity and $Z = 0.008$ models are within the observed range of Se and Kr PN abundances. Starting with a scaled solar abundance distribution, with $[s/O] = 0$, it is not possible to obtain sub-solar Se abundances, i.e., $[\text{Se}/\text{O}] < 0$. Likewise, the most Kr-enriched objects, with $[\text{Kr}/\text{O}] > 1$, are also not matched by the models.

The boxes indicating the range of derived PN abundances are somewhat misleading, because they do not convey the Se and Kr abundance distribution of PN, and most importantly, the number with extreme Se and Kr abundances. Fig. 4 from SD08 shows that there are only six PN out of 120 with low Se abundances, that is $[\text{Se}/\text{O}, \text{Ar}] < -0.3$. There are also only six PN with high Kr abundances, that is $[\text{Kr}/\text{O}, \text{Ar}] > 1$. Indeed, the rest of the sample of 120 PNe shows $[\text{Se}/\text{O}, \text{Ar}]$ between 0 and 1, consistent with the stellar models. Likewise, most of the Kr-enriched PN have $0 \lesssim [\text{Kr}/\text{O}, \text{Ar}] \lesssim 1.0$, consistent with the AGB mod-

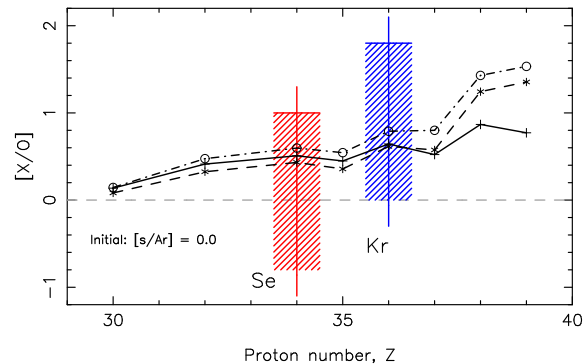


Figure 3: The surface abundances of neutron-capture elements around the first *s*-process peak. The solid line indicates abundances for the $3M_{\odot}$, $Z = 0.02$ model, the dashed line abundances for the $2.1M_{\odot}$, $Z = 0.008$ model, and the dot-dashed line abundances for the $2.5M_{\odot}$, $Z = 0.008$ model. Abundances are taken at the tip of the TP-AGB, after the last computed thermal pulse. The boxes represent the range of observed Se and Kr abundances for the full PN sample, see text for details.

els plotted in Fig. 3. There are still large uncertainties in deriving the Kr and Se abundances from PNe spectra. Hence it is possible that the most extreme PN abundances are effected by these uncertainties.

Finally, one other possibility is that the PN with the lowest Se abundances do not reflect internal nucleosynthesis during the progenitor AGB phase, but the initial Se abundance. Hence the very low Se/O abundances are the result of a peculiar galactic chemical evolution. If this is the case, then it would be intriguing to see if chemical evolution models would be able to explain the large spread in Se found in the full sample of PNe.

4 Low-metallicity PN

There have been a few low-metallicity PN identified including BoBn 1 (Otsuka et al. 2008; Zijlstra et al. 2006). These PN likely originate from low-mass progenitors with initial masses less than $\sim 1M_{\odot}$. These PN could be used as tracers of the low-metallicity environment out of which the progenitor stars formed, and they could be used to constrain the evolution and nucleosynthesis of low-metallicity AGB stars.

In Fig. 4 we show the *s*-process abundance distribution for two low-metallicity, low-mass AGB models. For these models we choose an initial α -enhanced abundance pattern (e.g., $[\text{O}/\text{Fe}] = +0.4$), which results in initial heavy element abundances with $[X/O] = -0.4$ when measured relative to oxygen. Note that relative to iron, the initial abundances for these elements are scaled solar, i.e., $[X/\text{Fe}] = 0$. In Fig. 4 we show the observed Se and Kr abundance distribution from the SD08 sample, noting that most of the PN used were Galactic PNe with higher metallicities than used in the AGB models presented here. From Fig. 4

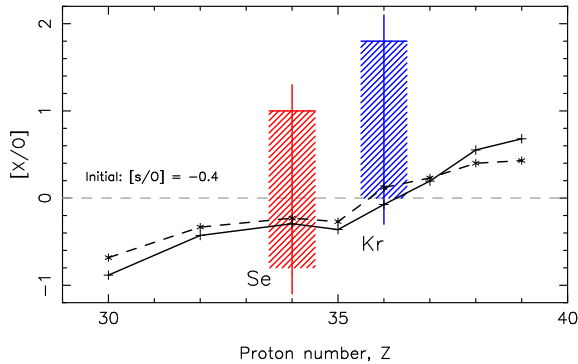


Figure 4: Same as Fig. 2, except the models shown are the $1.25M_{\odot}$, $[\text{Fe}/\text{H}] = -2.3$ model (solid line), and the $2M_{\odot}$, $[\text{Fe}/\text{H}] = -2.3$ model (dashed line). An α -enhanced initial abundance pattern was used (e.g., $[\text{O}/\text{Fe}] = +0.4$), and scaled solar for elements heavier than iron.

we see that the relative ratio of Zn/O is sub-solar, with $[\text{Zn}/\text{O}] \sim -1$ (starting at $[\text{Zn}/\text{O}] = -0.4$) from both models. If we examine the oxygen abundance, we find that a significant amount of this element is dredged to the surface, that is, $[\text{O}/\text{Fe}] = 0.87$ for the $1.25M_{\odot}$ model, and $[\text{O}/\text{Fe}] = 1.20$ for the $2M_{\odot}$ case. In both cases, Zn is actually produced by the s -process but in smaller quantities to oxygen, hence the $[\text{X}/\text{O}]$ ratios do not reflect the degree of production. For example, the final $[\text{Zn}/\text{Fe}] = 0.45$ for both models. Note that in both models, the iron abundance remains essentially unchanged.

Likewise for Kr, the abundances measured relative to iron are $[\text{Kr}/\text{Fe}] = 1.0$ dex and 1.1 dex for the $1.25M_{\odot}$ and $2M_{\odot}$ models, respectively. This is compared to $[\text{Kr}/\text{O}] \approx 0$ (see Fig. 4). Hence our results indicate that for the lowest metallicity PNe, the dredge-up of oxygen implies that this element is no longer a suitable proxy for the initial metallicity of the progenitor star. Argon is sometimes used in place of oxygen (Leisy & Dennefeld 2006, SD08), under the assumption that it remains unchanged by AGB nucleosynthesis. In Karakas et al. (2009) we showed that this is indeed the case. Zinc is also a potentially useful reference element because it does not condense into dust as easily as iron (e.g., Welty et al. 1999), and can be observed in PNe (Dinerstein & Geballe 2001). Zn is at the beginning of the s -process chain, and our results show that it can be produced in observable quantities in low-metallicity AGB stars. The best indicator of the metallicity is iron, but the element iron abundance is difficult to accurately determine from PN spectra (Perinotto et al. 1999; Sterling et al. 2005; Delgado Inglada et al. 2009).

5 Concluding Remarks

Abundances derived from PN spectra are an invaluable tool to study the late phases of stellar evolution of low and intermediate-mass stars, as well as trace the chem-

ical evolution of galaxies. Elemental abundances for C, N, O, S, the noble gases He, Ne, and Ar, as well as elements produced by neutron capture processes including Ge, Se, Kr, and Ba can be obtained, with varying degrees of accuracy. Observations of neutron capture elements in PNe can be used to constrain the amount of third dredge up mixing following the final thermal pulses of the progenitor star. In Karakas et al. (2009) we attempted to use the Se and Kr abundance information for Type I PNe, along with information on lighter element abundances (e.g., C, N, O, Ne etc) to constrain the neutron source operating in intermediate-mass AGB stars. We were unable to reach firm conclusions using the Se and Kr abundances. Certainly, it seems that the ^{22}Ne source is required to produce enrichments in s -process elements in these more massive AGB stars. It is less clear if the ^{13}C neutron source is also required. Increases in the Kr abundances were observed in models with a ^{13}C pocket, but not beyond the amounts observed in Type I PN spectra. Obtaining abundances for more heavy elements beyond the first s -process peak may help to distinguish among the possibilities.

Type I PNe may also originate from binary interactions, and/or by rapid rotation during the progenitor's main sequence phase. Certainly obtaining more abundances for Type I PNe may help to distinguish between the single or binary evolutionary channels, and to constrain the initial progenitor masses of these systems.

We compared results from lower mass AGB models to the full sample of PNe from SD08. Our results indicate that AGB models of solar or near solar metallicity produce a reasonable match to Se and Kr enrichments seen in the full sample. Our models cannot explain the PNe with sub-solar Se abundances, nor the PNe with the largest Kr enrichments. These outliers are only a small percentage of the full sample ($\sim 5\%$), and may reflect either uncertainties in the abundance determinations or the effects of inhomogeneous chemical evolution.

Finally, we present results for low-mass, low metallicity AGB models with metallicities appropriate for the Halo ($[\text{Fe}/\text{H}] \approx -2.3$). These AGB models were computed with an α -enhanced initial composition, and scaled solar for elements heavier than iron. In these low-metallicity AGB models, oxygen is dredged-up to the surface, which means that measuring the enrichment of heavy elements relative to this element (e.g., $[\text{Zn}/\text{O}]$) produces misleading results. For example, $[\text{Zn}/\text{O}] \approx -1$ for these models, when $[\text{Zn}/\text{Fe}] \approx 0.45$. Hence, it is important to determine the level of O dredge-up occurring, or to use another, more suitable proxy for the metallicity (e.g., Ar or Fe if possible).

Acknowledgments

The authors would like to thank Quentin Parker for organising the MASH workshop, and for his patience in waiting for this paper! AIK acknowledges support from the Australian Research Council's Discovery Projects funding scheme (project number DP0664105). ML is supported by the Monash Research Fellowship.

References

- Aller, L. H. & Czyzak, S. J. 1983, *ApJS*, 51, 211
- Boothroyd, A. I. & Sackmann, I.-J. 1999, *ApJ*, 510, 232
- Busso, M., Gallino, R., & Wasserburg, G. J. 1999, *ARA&A*, 37, 239
- Corradi, R. L. M. & Schwarz, H. E. 1995, *A&A*, 293, 871
- Delgado Inglada, G., Rodríguez, M., Mampaso, A., & Viironen, K. 2009, *ApJ*, 694, 1335
- Dinerstein, H. L. & Geballe, T. R. 2001, *ApJ*, 562, 515
- Dopita, M. A., Vassiliadis, E., Wood, P. R., Meatheringham, S. J., Harrington, J. P., Bohlin, R. C., Ford, H. C., Stecher, T. P., & Maran, S. P. 1997, *ApJ*, 474, 188
- Gallino, R., Arlandini, C., Busso, M., Lugaro, M., Travaglio, C., Straniero, O., Chieffi, A., & Limongi, M. 1998, *ApJ*, 497, 388
- García-Hernández, D. A., García-Lario, P., Plez, B., D'Antona, F., Manchado, A., & Trigo-Rodríguez, J. M. 2006, *Science*, 314, 1751
- Herwig, F. 2005, *ARA&A*, 43, 435
- Karakas, A. I. & Lattanzio, J. C. 2007, *PASA*, 24, 103
- Karakas, A. I., Lugaro, M., & Gallino, R. 2007, *ApJ*, 656, L73
- Karakas, A. I., van Raai, M. A., Lugaro, M., Sterling, N. C., & Dinerstein, H. L. 2009, *ApJ*, 690, 1130
- Lambert, D. L., Smith, V. V., Busso, M., Gallino, R., & Straniero, O. 1995, *ApJ*, 450, 302
- Leisy, P. & Dennefeld, M. 2006, *A&A*, 456, 451
- Magrini, L., Stanghellini, L., & Villaver, E. 2009, *ApJ*, 696, 729
- Moe, M. & De Marco, O. 2006, *ApJ*, 650, 916
- Otsuka, M., Izumiura, H., Tajitsu, A., & Hyung, S. 2008, *ApJ*, 682, L105
- Perinotto, M., Bencini, C. G., Pasquali, A., Manchado, A., Rodríguez Espinosa, J. M., & Stanga, R. 1999, *A&A*, 347, 967
- Sharpee, B., Zhang, Y., Williams, R., Pellegrini, E., Cavagnolo, K., Baldwin, J. A., Phillips, M., & Liu, X.-W. 2007, *ApJ*, 659, 1265
- Stanghellini, L., Guerrero, M. A., Cunha, K., Manchado, A., & Villaver, E. 2006, *ApJ*, 651, 898
- Stanghellini, L., Shaw, R. A., Balick, B., & Blades, J. C. 2000, *ApJ*, 534, L167
- Sterling, N. C. & Dinerstein, H. L. 2008, *ApJS*, 174, 158
- Sterling, N. C., Dinerstein, H. L., Bowers, C. W., & Redfield, S. 2005, *ApJ*, 625, 368
- Truran, J. W. & Iben, Jr., I. 1977, *ApJ*, 216, 797
- van Winckel, H. 2003, *ARA&A*, 41, 391
- Welty, D. E., Hobbs, L. M., Lauroesch, J. T., Morton, D. C., Spitzer, L., & York, D. G. 1999, *ApJS*, 124, 465
- Zijlstra, A. A., Gesicki, K., Walsh, J. R., Péquignot, D., van Hoof, P. A. M., & Minniti, D. 2006, *MNRAS*, 369, 875